Nanoscale Res Lett (2010) 5:1182–1189
DOI 10.1007/s11671-010-9623-0

NANO EXPRESS

Creation of Controlled Defects Inside Colloidal Crystal Arrays with a Focused Ion Beam

Simone Magni · Marziale Milani

Received: 11 February 2010 / Accepted: 28 April 2010 / Published online: 12 May 2010

Abstract In this work the reliability of the focused-ion-beam (FIB) patterning on polystyrene (PS) colloidal crystals at different scales is determined. Ordered arrays of PS spheres (465 nm) are successfully modified by selectively removing a single sphere. The water-vapor assisted FIB milling is crucial to obtain this result. Furthermore, isolated PS spheres are FIB drilled with or without chemically enhanced milling aiming at the exploration of the limits of such a technique. These controlled defects created using the FIB-assisted techniques may be helpful in preparing mockups of photonic crystals, sensors or as colloidal masks for diverse lithographic processes.

Keywords (Ion-assisted) Lithography · Positive-ion beams · Ion-beam impact interactions · Colloidal system · Photonic band gap materials

Introduction

Ordered aggregates of colloidal spheres of different sizes (from 50 nm to 2 μm) and compositions (e.g., PS, SiO_2 among others) are employed in the construction of devices having different applications in nanotechnology. Films of colloidal spheres can be used e.g., as masks in imprint contact lithography [1], dry etching lithography [2] or directly as 'focusing lens' in nanosphere photolithography [3, 4] in order to fabricate arrays for sensing devices or surface plasmon-polariton (SPP) structures. Spheres stacked in some layers and infiltrated by a suitable light-transmitting media can be employed as direct opal (DO) photonic crystals (PC's) [5, 6]. Moreover, arrays of colloidal spheres are commonly used as templates for inverted opals (IOs), which can work as PC's or as gas sensors [6, 7, 8].

Masks in which the absence of the colloidal particles is controlled can provide a 'superimposed' geometry to the structure one can normally only achieve by standard self-assembling. The possibility of achieving controlled defects in the structure is of paramount importance for all these applications. For example, the absence of a sphere (point defect) can be used as an optical cavity or a selective site. A linear defect such as a missing row of spheres can provide a waveguiding structures inside conventional DO PC's or SPP PC's.

Many techniques have been employed to achieve such controlled defects, mainly involving topdown approaches [9, 10, 11, 12, 13, 14]. In Ref. [9], deterministic defect sites in DO's formed by PMMA microspheres have been introduced by means of electron beam lithography and the subsequent development in methyl isobutyl ketone. CdS hollow spheres have been completely removed or partially drilled with a long-time exposure to a high-current electron beam in a gas atmosphere (N_2, H_2O) [11].

The laser ablation produced by a femtosecond IR laser has been shown to achieve a single-sphere removal in a monolayer of 1-μm silica spheres [12]. Point defects can be also precisely introduced with other methods. The authors of Ref. [10] have used a multistep process which includes the spin-coating and the the nano-imprinting of a PMMA

S. Magni (✉)
Scottish Universities Physics Alliance, School of Physics and Centre for Science at Extreme Conditions, University of Edinburgh, Edinburgh EH9 3JZ, UK
e-mail: simone.magni@ed.ac.uk

M. Milani
Department of Materials Science and Laboratory FIB/SEM 'Bombay', University of Milano-Bicocca, Via Cozzi 53, 20125 Milan, Italy

resist on top of a silica DO, the insertion of smaller SiO_2 spheres (defects), the removal of the resist and the final re-growth of the silica opals. Finally, a monolayer of PS colloidal particles with tunable cavity dimensions has been produced by partially embedding the particles with electrochemically deposited nickel, drilling the cavities with Reactive Ion Etching (RIE) and removing the nickel by means of wet etching [14].

The Focused Ion Beam (FIB) is a tool capable of subtractive (milling) and additive (deposition) fabrication on a submicrometer scale and is employed most often in top-down nanotechnology [15, 16, 17, 18, 19]. Recently, it has been also utilized to drill SiO_2 colloidal spheres [13] and mill pits in SiO_2 colloidal aggregates [20].

The aim of this work is to show how such a technique can be used in a similar fashion to the work in Ref. [13] on polymeric colloidal crystals. Further, we will show how the water-vapor enhanced milling could be advantageous in this case and what the limits of FIB milling in relation to the geometry one would like to achieve are. Some preliminary results were presented in the conference paper Ref. [21], here our findings are presented in full.

The paper is organized as follows: in Sect. 2 we describe the techniques we have used for milling, imaging and estimation of the diameter of the drilled features. In Sect. 3 we report the results on the selective removal of a single sphere in ordered PS colloidal arrays and the drilling of through holes or circular cavities (nonthrough holes). These results are discussed in Sect. 4. In Sect. 5 we present our conclusions.

Experimental

Commercial PS spheres (TAAB Ltd, London, UK) suspended in distilled water and having a diameter of 465 nm are deposited on a silicon surface. A SEM survey of a large number of spheres after the aggregation proves that their diameter is within a 2% confidence limit. In this work, we consider regular portions of selfassembled DO's on silicon obtained by evaporation method from such PS colloidal spheres.

We have made use of a Quanta 3-D 200 DualBeam workstation (FEI Europe B.V., Eindhoven, Netherlands) coupling a FIB with an Environmental Scanning Electron Microscope (ESEM), used for both the modification and the imaging of the altered structures. Colloidal crystals formed by submicrometer spheres are inherently nonconductive and charge builds up when irradiated by charged particle beams. The deposition of a conductive layer has been previously adopted as a countermeasure to avoid charging during either electron imaging or FIB milling operations on SiO_2 particles [13]. In our case this operation reveals itself unnecessary and the removal of even the thinnest conductive layer may be impossible without damaging the underlying structure.

Charging-free images with good contrast and resolution have been obtained working with the ESEM modality at an acceleration voltage of 15 kV and at gas pressures (water vapor) of 200–220 Pa. We have also achieved a good resolution with secondary electron (SE) imaging by adopting the FIB as a primary beam and at the lowest ion current (1 pA).

Aiming at the removal or the drilling of the PS sphere, we have extensively used the circular pattern milling where the disk-like shape to be carved is approximated by a series of beam-spots arranged along concentric circles [22]. The beam dwell time is set to 1 μs with a spot overlapping of 50% along both radial (R) and tangential (T) directions. This overlapping corresponds to a pitch of 3.5 nm both in R and T directions while working at 1 pA ($\sim$7 nm FWHM beam diameter) and milling disks of 30–500 nm in diameter. The patterning strategy is circular scanning where the milling is started at the center and then carried out from the center to the outer circles up to the value of the chosen diameter.

In some experiments we have used water-vapor assisted milling, namely the FEI Selective Carbon Milling (SCM), in order to speed up the milling rate of PS. This method consists of locally delivering H_2O vapor on the sample surface providing a chemically enhanced (CE) FIB milling for carbon-based materials [23]. Typical vacuum pressures in the chamber increase from a few 10^{-4} Pa up to a few 10^{-3} Pa while the water vapor is injected at a lower pressure than ESEM on the milling site by means of a dedicated extensible capillary.

SCM is faster than standard milling because of the increased sputter yield of PS due to CE milling. SCM is programmed by default with an increased pitch of the patterning allowing a shorter loop time (i.e. the time interval required for the beam to raster the programmed pattern once). This milling recipe also sets the overlapping at 0%, the relative interaction diameter at 99%, i.e. a pitch of 13.5 nm along R and T for currents of 1 pA, while the dwell time is kept at 1 μs. The lower ion dose allowed by this recipe reduces the side effects as e.g., charging, amorphization, structural damaging, ion implantation, etc.

The diameter of the carved features have been estimated in both the vertical and the horizontal directions from diverse ion and electron images with an edge detection technique on the gray level of the digital pictures (cf. [24, 25] for further details). Holes drilled with the same recipe have been considered along with different images and the two different directions in order to have adequate statistics to calculate the mean value and the standard deviation, σ.

At least eight measures per diameter are used to estimate σ which is used as the error bar in the plot shown in Fig. 4 (right). In our case σ also accounts for systematic errors that may arise from the ultimate resolution of the images (3.5 nm for ESEM and 5 nm for the FIB imaging), the imperfect alignment of the drilling axis and the sphere axis, etc.

Results

The possibility of FIB-assisted micromanipulation of PS colloidal particles has been explored. Many tests have been arranged on isolated PS spheres (Fig. 1 left). Circular milling patterns with a diameter of 500 nm can remove a single, isolated PS sphere. M1 in Fig. 1 (left) shows a successful result (circular pattern $\varnothing = 500$ nm, standard milling, dose 3.30 nC/μm^2, total time t_m = 661 s). However, results are not completely reproducible since sometimes charge builds up on the milled sphere causing a drift of the incoming ions (cf. e.g. M3, same parameters as M1).

To prevent charging one might employ the technique reported by Stokes et al. [26], regarding the charge neutralization by means of the defocused SEM in spot mode. The electron beam acceleration is kept at 1 kV and current and defocusing length are set to satisfy Eqs. (3), (5) and (8) of the above mentioned work. However, in our situation such a technique seems to destabilize the milling even more because many incoming flooding electrons may increase the electrostatic potential of the sphere with respect to the substrate (see M2 in Fig. 1 (left)). To check whether these electrons may be responsible for a charge destabilization, another milling is conducted in the absence of the neutralization but with a SEM image taken after one half of the milling time. The result is reported in M4–Fig. 1 (left), where a similar effect to M2 can be seen.

More complex milling patterns have been tested. In S1–Fig. 1 (right) we show an attempt carried out combining the drilling of a small cavity (circular pattern $\varnothing = 100$ nm, standard milling, dose 2 nC/μm^2) with an annular patterning (internal diameter $\varnothing_1 = 100$ nm, external diameter $\varnothing_2 = 400$ nm, standard milling, dose 1.33 nC/μm^2) for a total time $t_m = 188$ s. A part of the sphere still remains unaffected after the milling.

SCM has been tested to reduce the milling time for a single sphere removal which may allow the FIB milling to compete with other techniques. SCM contributes to the decrease of the milling time as discussed in Sect. 2 and in [23]. A lower ion dose (50% or less) to obtain the same milling depth also results in an overall slighter charging, avoiding unwanted drift. In S2–Fig. 1 (right) the removal of a PS microsphere is achieved at 1 pA by means of the SCM with a circular pattern $\varnothing = 500$ nm and a dose of 1.66 nC/μm^2($t_m = 332$s). However, the pattern diameter can be reduced in order to save time without affecting the final results. A circular pattern with $\varnothing = 190$ nm and a dose of 1.66 nC/μm^2 with a milling time t_m of 50 s can achieve similar results (see S3 in the inset of Fig. 1 (right)), obtaining a greater advantage than in the previous case (282 s less). In both the pictures of Fig. 1 (right) one can also clearly see the 'footprint' of the removed sphere.

The same study in terms of the diameter and the dose has been carried out on selfassembled spheres. The results on a DO are shown in Fig. 2a. The diameter of the circular milling is reduced from 350 to 200 nm while the dose is kept constant at 1.66 nC/μm^2 (top row and middle row,

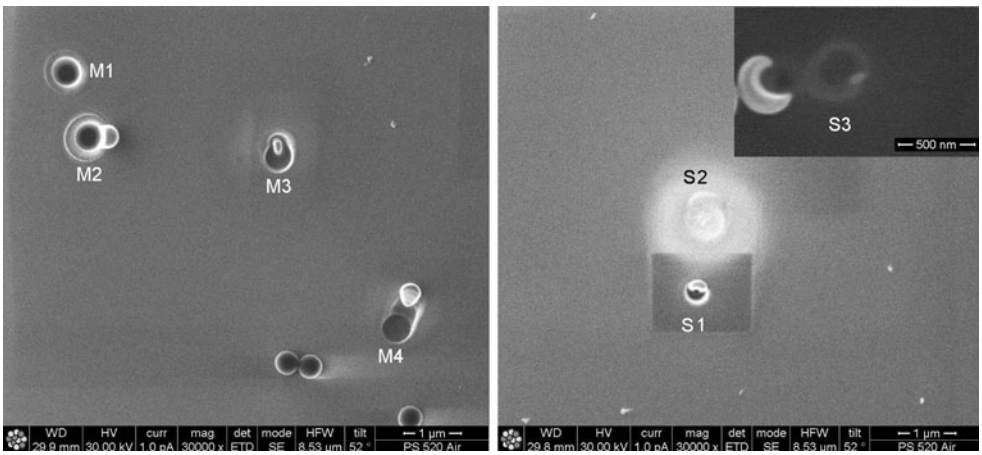

Fig. 1 *Left*: Attempts to achieve a single-sphere removal using different strategies with a standard FIB milling (i.e., without water vapor injection for CE milling). The recipes for M1,M2, M3 and M4 are reported in the text. *Right* S1: Another attempt to achieve a single-sphere removal without SCM; S2: a successful attempt which employs the SCM option. In the inset, S3: a further improvement of the recipe in S2 that achieves the sphere removal in 50 s (Both ion images with a Horizontal-Field Width [HFW] of 8.53 μm; inset: ion image, bar 500 nm)

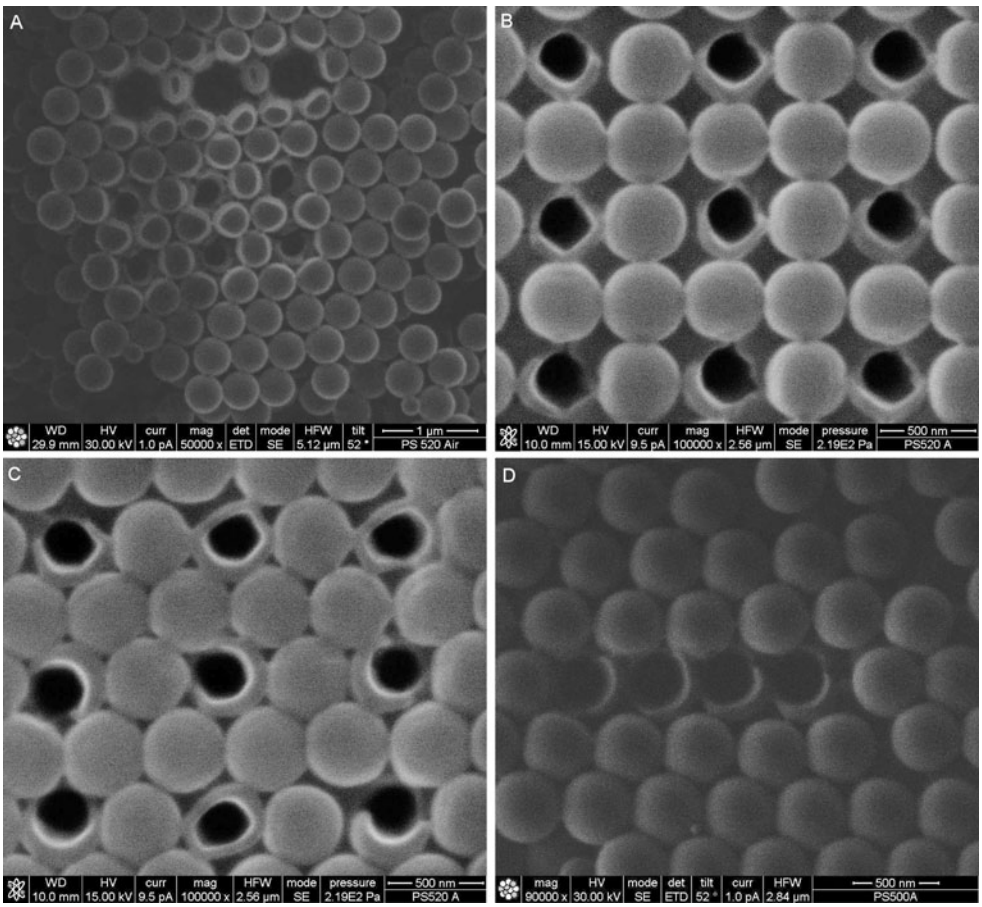

Fig. 2 **a** Selective removal of PS spheres to obtain an alternating geometry: three attempts (from *top* to *bottom*) to refine the recipe which employs the water-assisted milling; **b** successful achievement in a square array; **c** results for a hexagonal array. **d** serial removal of spheres in a row to obtain a waveguide-like optical cavity. (**a** and **d**: ion images, HFW = 5.12 μm and HFW = 2.84 μm, respectively; **b** and **c**: ESEM at 15 kV, chamber pressure 220 Pa, HFW = 2.56 μm both)

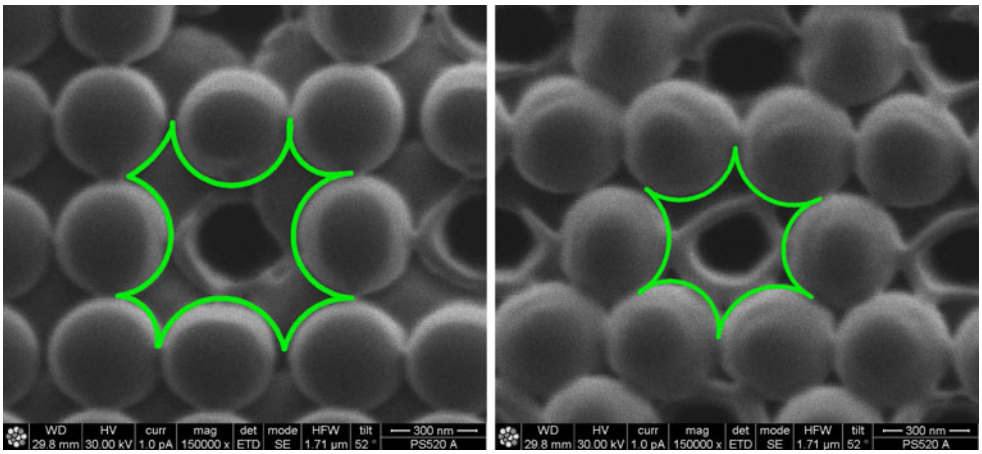

Fig. 3 Close-up views of: (*Left*) the sphere removal in the square array of Fig. 2b; The area circumscribed by the *green curve* is $\left(4-\frac{3}{4}\pi\right)d^2$ where d is the sphere diameter. *Right*: The same operation but in the hexagonal array of Fig. 2c; here the circumscribed area is $\left(3-\frac{\pi}{2}\right)d^2$. The effect of redeposition changes by switching from a square to a hexagonal array. (Both ion images with HFW = 1.71 μm)

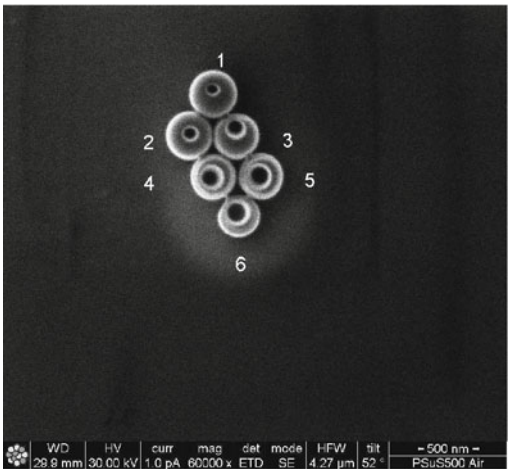

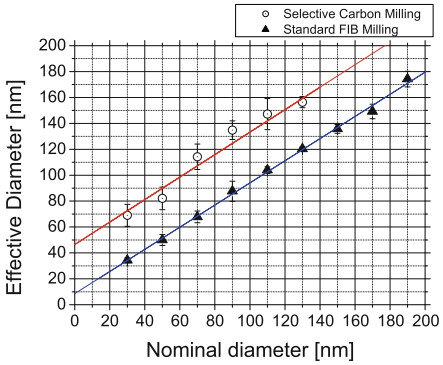

Fig. 4 (*Left*): A series of holes drilled by FIB at 30 kV with 1 pA nominal current (circular pattern, SCM); the nominal diameters are 30, 50, 70, 90, 110 and 130 nm, respectively, from 1 to 6 (Ion image: HFW = 4.27 µm). *Right*: a plot reporting the nominal vs. the measured diameters of the drilled features (*open circles* with SCM, *black diamond* without SCM); the error bars are the standard deviations calculated considering both different measures of the same hole and different drilled holes; for the standard FIB milling (*blue line*) a linear interpolation has the slope of 0.85 ± 0.02 and the intercept of 9 ± 2 nm; for SCM (*red line*) the slope is 0.87 ± 0.08 and the intercept is 46 ± 8 nm.

respectively, in Fig. 2a). In this case, the milling time is decreased from 169s to 60s per single-sphere removal and the damage on the spheres closest to the produced vacancy is also minimized. A milling time down to 48 s/sphere can be achieved by further reducing the dose to 1.33 nC/µm^2 and the diameter to 190 nm (bottom row in Fig. 2a).

Results of periodic removals on 2-D square and hexagonal arrays are displayed in Fig. 2b, c with the recipe we have just described. A comparison between the hexagonal and the square array is useful to understand that the presence of the nearest neighbors is not negligible in the removal operation. The packing configuration due to six nearest neighbors instead of four is affected by a more considerable redeposition than it is in the latter case (cf. Fig. 3 (left, right)). This effect is independent from the thickness of the colloidal crystal being observed both on monolayers and 3-D crystals with a different number of layers (results not shown here). The single-sphere removal technique can obtain different geometries such as the alternated vacancies reported in Fig. 2b, c or the removal of a row of spheres in Fig. 2d.

To obtain better knowledge of the interaction between the ion beam and PS spheres when SCM is being employed, isolated small clusters have been FIB drilled by performing circular patterns with smaller radii (Fig. 4 (left)). Holes with nominal diameters in the range of 30–150 nm with SCM and 30–190 nm without SCM have been drilled, at the fixed dose of 1.66 nC/µm^2.

The upper limit originates from the fact that the drilled holes start to be asymmetric for diameters larger than 150 nm (200 nm without SCM) because of charge drift and/or mechanical drift of the sample stage (both these effects increase with larger milling time). The typical result is a half-moon shaped particle rather than a symmetric 'nanobead'. In the inset of Fig. 1 (right) a typical result is shown on a sphere drilled using SCM and a nominal diameter of 150 nm.

The lower limit of 30 nm is set because it is at the edge of the ultimate resolution of the FIB micromachining of PS spheres. In the case of the standard milling an actual diameter of 30 nm is still obtained for smaller starting nominal diameters (a similar limit of 80 nm is reported in [13]). When using SCM, the input diameter of 30 nm corresponds instead to a pattern formed by four beam spots arranged in a cross.

The effect of SCM on PS reflects on an actual larger hole than the nominal diameter that is input in the FIB-SEM workstation (Fig. 4 (right)). A linear fit quantifies a systematic increase of the diameter in 46 ± 8 nm (intercept of the best fit) with a slope close to one (0.87 ± 0.08). The same calculation for the standard milling gives 9 ± 2 nm and again a slope close to one (0.85 ± 0.02). The latter proves that the systematic increase is real and not due to a misleading calibration or to the way in which the diameters have been estimated.

SCM can also be employed to more effectively achieve a through hole because it allows a larger depth (z)/diameter (d) aspect ratio ($\frac{z}{d}$). Indeed, from Fig. 5 (right) one cannot be sure that the cavity drilled at 60 nm is actually boring through while it is evident for the 100 nm hole (cf. the small holes in the substrate).

Figure 5 (left) displays through holes with nominal diameters of 60, 90, 120 nm obtained inside the colloidal spheres albeit with larger effective diameters. Further,

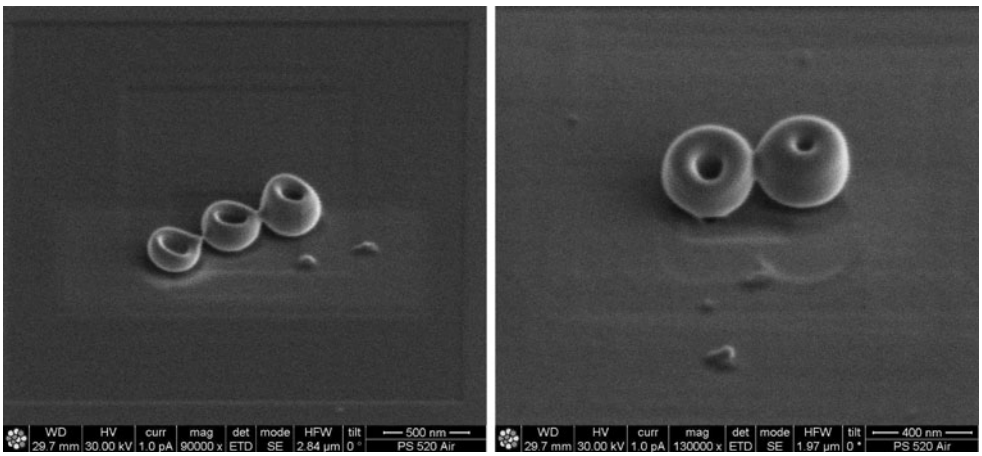

Fig. 5 Nanocavities obtained by FIB drilling at 30 kV with 1 pA nominal current. *Left figure*: a circular pattern with SCM used to drill cavities with nominal diameters of 60, 90 and 120 nm, respectively (from *right* to *left*). *Right figure*: a circular pattern with serial milling with a through hole of 100 nm (*left*) and a circular cavity of 60 nm (*right*), respectively. (Ion images HFW 2.84 µm and 1.97 µm)

SCM introduces a 'plastic deformation' in the drilled particles especially when very large cavities are drilled. In these extreme cases, SCM confers a toroidal shape to them as opposed to the 'bead-like' shape generated at the smallest diameters. An unwanted asymmetry is also present and it could be related to the direction of the flux of the water vapor utilized during the CE milling.

Discussion

We have presented the issue of manipulating colloidal crystals at the level of their elemental building blocks. This has been previously obtained by different electron beam lithographies [9, 11] or by femtosecond-laser machining [12]. FIB can compete with such techniques when SCM is employed to dramatically increase the milling rate. In the case of PS spheres (diameter 465 nm) the removal of one sphere takes 48 s with a circular pattern of 200 nm, at the current of 1 pA and the dose of 1.33 nC/µm^2.

The feasibility of milling PS spheres suggests the possibility of a geometry selection with a FIB on both colloidal masks (monolayers) and colloidal crystals (with 2-D or 3-D structures). The damage beneath the modified layer is minimized by carefully choosing the dose, i.e. the nominal depth on the software of the FIB/SEM workstation (cf. Fig. 2b, c). Some debris due to the milling operation can still be present with a complication relative to the hexagonal arrays. This is due to a larger redeposition that appreciably occurs in the presence of a more packed configuration (compare Fig. 3 (left and right)), which may require a further polishing in the zone of the debris.

A quantitative estimation of redeposition has been previously sketched in the simple trench geometry (cf. Ch.6 in [15], Ch.2 in [17] and [27]). In our case, we can only qualitatively explain how the more confining geometry of the hexagonal packing can affect the kinetics of the redeposition. Using geometrical considerations (Fig. 3), the projected areas of the created vacancies are $\left(4-\frac{3}{4}\pi\right)d^2$ and $\left(3-\frac{\pi}{2}\right)d^2$ in the square array and in the hexagonal one respectively (d is the sphere diameter). The enclosed volume of the vacancy may be approximated by this area times d. This volume is smaller by about 15% in the hexagonal-packing case than it is in the square-packing case.

Bearing in mind the increased pressure mechanism for redeposition [17], we can expect that the localized pressure increases faster and reaches a higher equilibrium value in this smaller volume than it does in the less confined situation. This ultimately results in a smaller mean free path of the sputtered atoms within this volume, multiplying the probability that a sputtered atom/sample collision results in redeposition. Moreover, the presence of six nearest neighbors at a distance d from the center instead of four provides a lateral surface which is larger by 50% and may increase further the chance that the ejected atoms stick again to the side walls of the vacated volume.

Nanocavities in silica nanospheres have been previously obtained by Woldering et al. [13] with a FIB. These authors report that CE etching using I_2 vapor has a negligible effect on the FIB drilling of silica at the nanometer scale. This is expected as the enhancement factor in this case is one (cf. e.g., Chap.3 in [17]). As a difference from this work, we note that on the contrary SCM introduces an interesting widening of the drilled hole due to the chemical action of the H_2O vapor on the PS spheres (Fig. 4-right). The systematic difference between nominal and actual diameter of the cavity is of 46 ± 8 nm which is about three times larger than the expected interaction diameter (14 nm). Indeed, it cannot be explained neither by

assuming only that of the beam at 1 pA doubles (from ~7 to ~14 nm) nor by taking into account the calibration of the system in the standard case. One should always evaluate this effect during the use of water-vapor injection to enhance the FIB milling on these scales.

The SCM may also give rise to a deformation of the sphere which departs from the circular shape (Fig. 5-left), displaying a common problem in CE-FIB milling [16]. However, the FIB-produced PS nanobeads may still undergo fewer deformations than those resulting from the three-step process (nickel deposition, RIE and wet etching) employed in Ref. [14].

Outlook and Conclusions

It has been shown how colloidal spheres can be drilled or selectively removed by FIB milling, suggesting interesting applications for these controlled defects. In particular we have shown the nontrivial result of employing CE-FIB milling to carve features in complex geometries well below the micrometer limit. This was often neglected in the past (see e.g., the discussion in [16]). Further work should be done to explore all the challenging possibilities of the FIB-assisted techniques on colloidal particles at a submicrometer scale. For example, the CE-FIB milling utilizing XeF_2 vapor may be as useful in dealing with SiO_2 colloidal crystals as SCM is in dealing with PS selfassembled spheres [20].

The selective removal can produce monolayers of spheres with a new geometry (Fig. 2b–c), that can be used as masks in dry etching, optical lithography or as templates for imprint contact lithography. In particular the production of novel SPP band-gap PC's containing point defect structures are possible [28], e.g., as a result of the controlled defects in the monolayer of colloidal particles that may form the fabrication mask and/or the dielectric interstice.

The PS DO crystals employed in this work display a pale white color and a weak iridescence. In air they do not show any photonic band-gap. However, if infiltrated by a solution with a matching refractive index and eventually by a dye, the DOs can exhibit optical stop bands and can be usable as tunable lasers [5]. Alternatively, the DO can be infiltrated by silicon, germanium, III-V semiconductors or a few chalcogenides and an IO PC's is obtained when the initial DO template is removed [6].

The controlled defects caused by a missing sphere (Fig. 2c) or a missing row (Fig. 2d) can be used respectively as an optical cavity or as an optical waveguide inside PC's in either DO or IO configurations. In both cases, an issue may be the viability of embedding such defects inside 3-D PC's and may be solved by only partially removing the sphere or drilling it. In this way the opal may be easily re-grown in a similar fashion to Ref. [10]. The drilled holes (Fig. 5 left and right) can not only set up optical nanocavities inside the colloidal crystal but also selective sites for (bio)molecules in a sensing device [29]. If circular cavities are generated, these can be used instead as microvials for biochemical microanalysis (as suggested in [14]).

Both through holes and circular cavities can be achieved by the FIB. However, a fine tuning of the parameters (circular pattern diameter, dose, etc.) in function of the dimensions and the materials is required toward this goal. Furthermore, FIB cross sectioning and SEM imaging may be used to check whether or not the milled cavity is boring through. A similar technique has been previously utilized to explore of the internal part of latex hollow particles [30].

Acknowledgments S.M. carried out this work under a grant of the M.I.U.R. (Italian Ministry of Education, Universities and Research) when he was at the Department of Materials Science, University of Milano-Bicocca, Italy. We would like to thank A.S. Campbell and J.E. Proctor (University of Edinburgh) for the revision of the English text. The following people are also acknowledged for fruitful discussion and/or joint work: F. Causa and F. Ghezzi (Istituto di Fisica del Plasma, CNR-EURATOM, Milan, Italy), F. Tatti and T. Vystavel (FEI Europe B.V.), D. Batani, H.E. Roman, R.A. Siliprandi (Department of Physics, University of Milano-Bicocca, Italy).

References

1. Z. Sun, B. Yang, Nanoscale Res. Lett. **1**, 46 (2006)
2. J.C. Hulteen, R.P.V. Duyne, J. Vac. Sci. Tech. A **13**, 1553 (1995)
3. W. Wu, D. Dey, O. Memis, A. Katsnelson, H. Mohseni, Nanoscale Res. Lett. **3**, 123 (2008)
4. W. Wu, D. Dey, O. Memis, A. Katsnelson, H. Mohseni, Nanoscale Res. Lett. **3**, 351 (2008)
5. M.N. Shkunov, Z.V. Vardeny, M.C. DeLong, R.C. Polson, A.A. Zakhidov, R.H. Baughman, Adv. Funct. Mat. **15**, 21 (2002)
6. C. Lòpez, Adv. Mater. **15**, 1679 (2003)
7. A. Blanco, E. Chomski, S. Grabtchak, M. Ibisate, S. John, S. Leonard, C. Lopez, F. Meseguer, H. Miguez, J.P. Mondia et al., Nature **405**, 437 (2000)
8. R.W.J. Scott, S.M. Yang, G. Chabanis, N. Combs, D.E. Williams,G.A. Ozin, Adv. Mat. **13**, 1468 (2001)
9. P. Ferrand, M. Egen, R. Zentel, J. Seekamp, S. Romanov, C. Torres, Appl. Phys. Lett. **83**, 5289 (2003)
10. Q. Yan, A. Chen, S.J. Chua, X. Zhao, Adv. Mater. **17**, 2849 (2005)
11. R. Xie, T. Skiguchi, D. Li, D. Yang, M. Jiang, J. Phys. Chem. B **110**, 1107 (2006)
12. W. Cai, R. Piestun, Appl. Phys. Lett. **88**, 111112 (2006)
13. L.A. Woldering, A.M. Otter, B.H. Husken, W.L. Wos, Nanotechnology **17**, 5717 (2006)
14. Q. Yan, F. Liu, L. Wang, J.Y. Lee, X. Zhao, J. Mater. Chem. **16**, 2132 (2006)

15. J. Orloff, M. Utlaut, L.W. Swanson, *High resolution focused ion beams: FIB and its applications*. (Kluver Academic Plenum, New York, 2003)
16. A.A. Tseng, Small **1**, 924 (2005)
17. L. Giannuzzi, F. Stevie (eds), *Introduction to focused ion beams*. (Springer, New York, 2005)
18. L. Miglio, M. Milani, S. Magni, Nanotechnology top-down: an introduction from microelectronic to micromachining applications. (Aracne Editrice, Rome, 2006)
19. D.J. Stokes, F. Morissey, B.H. Lich, J. Phys. Conf. Ser. **26**, 50 (2006)
20. J. Moran, P. Wheat, J. Posner, Langmuir **24**, 10532 (2008)
21. S. Magni, M. Milani, F. Tatti, C. Savoia, J. Phys. Conf. Ser. **126**, 012059 (2008)
22. W. Hopman, F. Ay, W. Hu, V. Gadgil, L. Kuipers, M. Pollnau, R. de Ridder, Nanotechnology **18**, 195305 (2007)
23. T. Stark, G. Shedd, J. Vitarelli, D. Griffis, P. Russel, J. Vac. Sci. Tech. B **13**, 2565 (1995)
24. M. Milani, C. Riccardi, D. Drobne, A. Ciardi, P. Esena, F. Tatti, S. Zanini, Scanning **27**, 275 (2005)
25. S. Magni, M. Milani, C. Riccardi, F. Tatti, Scanning **29**, 185 (2007)
26. D.J. Stokes, T. Vystavel, F. Morissey, J. Phys. D Appl. Phys. **40**, 874 (2007)
27. H. Kim, G. Hobler, A. Lungstein, E. Bertagnolli, J. Micromech. Microeng. **17**, 1178 (2007)
28. S.I. Bozhevolnyi, Phys. Rev. Lett. **86**, 3008 (2001)
29. M.R. Gelfand, L. Bruderer, H. Mohseni, Opt. Lett. **34**, 1087 (2009)
30. E. Beach, M. Keefe, W. Heeschen, D. Rothe, Polymer **46**, 11195 (2005)